ON THE DETAILED DESIGN OF A QUASI-ZERO STIFFNESS DEVICE TO ASSIST IN THE REALISATION OF A TRANSLATIONAL LANCHESTER DAMPER

G. Gatti[a*], A.D. Shaw[b], P.J.P. Gonçalves[c], M.J. Brennan[e]

[a] *Department of Mechanical, Energy and Management Engineering, University of Calabria, Rende, Italy*

[b] *College of Engineering, Swansea University, Swansea, UK*

[c] *Department of Mechanical Engineering, Faculty of Engineering, UNESP, Bauru, Brazil*

[d] *Department of Mechanical Engineering, Faculty of Engineering, UNESP, Ilha Solteira, Brazil*

* Corresponding author:

G. Gatti, Department of Mechanical, Energy and Management Engineering, University of Calabria, Via P. Bucci 46C, 87036 Rende (CS), Italy – email: gianluca.gatti@unical.it

No. of figures: 18

No. of animations 2

No. of tables: 2

Abstract

A translational Lanchester damper is a device that adds damping to a structure at a point using a series combination of a viscous damper and a mass. The problem in the practical realisation of such a device is that a stiffness is required to support the mass, which changes the dynamic behaviour of the device, introducing a resonance frequency due to the interaction of the stiffness and inertia forces. This is a dynamic vibration absorber. To achieve a device that behaves broadly as a Lanchester damper rather than a dynamic vibration absorber, a very low stiffness is required, and this is the focus of this paper. The low stiffness is realised using a combination of linear springs and rigid links arranged with specific geometry into a compact device. Although the geometric configuration of the components leads to an inherently nonlinear device, the aim is to limit its working condition and exploit the linear-like behaviour. To this end, how the geometry affects the nonlinear behaviour is studied in detail, providing general guidelines for its design. A prototype Lanchester damper incorporating the low stiffness element was manufactured and tested on a single mode and two multi-modal vibrating structures.

Keywords: vibration absorber; vibration neutraliser; nonlinear energy sink; essentially nonlinear stiffness; high-static-low-dynamic-stiffness; passive vibration control.

1 Introduction

More than a century ago, Lanchester invented a torsional vibration damper for the crankshaft of an internal combustion engine [1]. This device, which involves a viscous damper and a rotating inertial mass, proved to be very effective [2] and is still in use today. It is called the Lanchester damper and has the advantage that it is effective over a wide range of frequencies, as it does not have a stiffness element, and is hence not tuned to a specific frequency. This, of course, is possible with a rotational device, and for a rolling device in the horizontal direction [3], but is impractical for a system that undergoes vertical translational motion because a spring is necessary to support the inertial mass. The addition of a spring completely changes the dynamic behaviour of the device, introducing a resonance due to the interaction of the stiffness and inertia forces. Ormondroyd and Den Hartog described this in detail in 1928 [4] and called the device a dynamic vibration absorber. Since then, there have been numerous articles on the dynamic vibration absorber, and it has been acknowledged as an effective vibration control measure used in a broad range of engineering applications encompassing civil, transport and aeronautical areas, for example [5,6]. It is sometimes called a tuned vibration absorber or a tuned mass damper, amongst others. The fundamental aim of this device, comprising mass, stiffness and damping is to add damping to a host structure, generally at a troublesome resonance frequency. If the objective is to suppress the forced harmonic response of the host structure, the dynamic vibration absorber is called a tuned vibration neutraliser, because the aim is vibration suppression at a single frequency, rather than the addition of damping.

In the past decade, there has been significant interest in improving the performance of the dynamic vibration absorber by introducing nonlinear stiffness, for example [7-9]. Design and optimization strategies have been investigated [10,11], and experimental approaches have been proposed for parameters identification [12]. In practice, springs cannot be extended/compressed to infinity, which involves nonlinear saturation stiffness issues [13,14]. Recent works on the use of nonlinear vibration absorbers include Godoy and Trindade [15], who investigated the tuning of a nonlinear dynamic vibration absorber based on a snap-through truss geometry, and Zou et al. [16], who proposed a geometrical device capable of customizing the nonlinear forces used for vibration isolation and energy sink devices.

If a dynamic vibration absorber has nonlinear stiffness, but a negligible linear stiffness (sometimes called an essentially nonlinear stiffness), then tuning in the classical way is not possible. Such a device is commonly referred to as a nonlinear energy sink, and has been studied by several researchers. It can broaden the frequency range at which it is effective [17-21], acting in a similar way to the Lanchester damper. However, suppose the nonlinear energy sink is subject to large amplitude vibrations, then effects due to the nonlinearity can appear [22-25], such as the existence of quasi-periodic motion, nonlinear amplitude jumps, and isolated detached branches of the frequency response curves. Many different configurations have been explored [26-29], and optimization strategies have been proposed [30,31].

This paper concerns the design of a device that behaves as a translational Lanchester damper over a broad range of frequencies, in a similar way to the nonlinear energy sink discussed above. A quasi-zero stiffness nonlinear spring [32] is designed to achieve this. It has a high-static and low-dynamic stiffness, similar to that exploited for vibration isolation problems [33,34]. The novelty lies in the design of the device, which exploits the combination of an articulated linkage and a pair of linear helical springs in tension, to achieve a quasi-zero stiffness effect. The work focuses on the design and implementation of a device operating in its linear regime rather than its optimisation, which has been covered in [35,36]. It builds on a previous article by the authors of this paper [37], in which an adjustable high-static and low-dynamic stiffness device was used to suspend masses on a multi-modal structure for ground vibration tests in the aerospace sector.

The paper is organised as follows. Following this introduction, Section 2 outlines the physical problem of adding damping to a host structure using a damping element and an inertial mass. Section 3 describes the proposed configuration of the translational Lanchester damper with quasi-zero stiffness, from the kinematic and quasi-static point of view, emphasising the limits for linear-like behaviour. A dynamic analysis of the device is carried out in Section 4, which highlights the fundamental theoretical performance and presents numerical validation by simulations. Section 5 describes the experimental work, which illustrates the behaviour of a prototype device attached first to a single degree-of-freedom system, and then on two different multi-modal engineering structures. The paper is then closed with some conclusions in Section 6.

2 Problem statement

There are many situations where it is necessary to add damping to a structure to reduce vibration at troublesome resonance frequencies. Sometimes this is done using unconstrained or constrained layer damping, where damping material is applied in a distributed manner to the structure [38,39]. In some cases, however, this is not possible, and damping is applied at a point. This is illustrated in Figure 1(a), where the host structure is represented as a dynamic stiffness K, and for convenience, the damping mechanism is assumed to be a viscous damper with damping coefficient c. In this figure, the damper has one end attached to ground, but this is not possible in many cases, so the ground is replaced by a mass as shown in Figure 1(b).

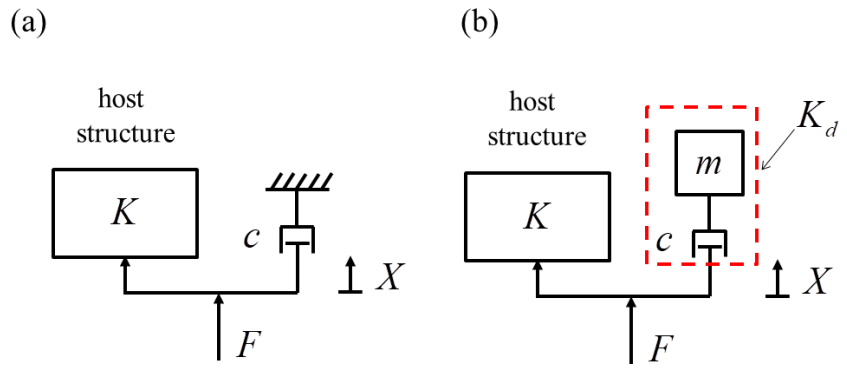

Figure 1. Schematic of a structure with dynamic stiffness *K* with (a) a damper connected to ground, and (b) a damper connected to a mass.

This changes the dynamic behaviour of the system significantly and can be investigated by noting that the dynamic stiffness of the complete system is given by

$$\frac{X}{F} = \frac{1}{K + K_d} \tag{1}$$

where *F* is the amplitude of the excitation force, *X* is the amplitude of the resulting displacement and K_d is the dynamic stiffness of the combination of the attached damper and mass. All the quantities are frequency domain variables. The dynamic stiffness of the attachment is seen to affect the response of the complete system. As mentioned above, the design requirement is that the attachment behaves as a damper, but this only occurs above a certain frequency. To determine this frequency, the dynamic stiffness of the attachment, which is a series combination of the damper and the mass, is studied. It is given by

$$K_d = \frac{1}{\frac{1}{\mathrm{j}\omega c} - \frac{1}{\omega^2 m}} \tag{2}$$

This can be rearranged to give

$$Z_d = \frac{K_d}{\mathrm{j}\omega} = \frac{\omega m c}{\omega m - \mathrm{j}c} \tag{3}$$

where Z_d is the impedance of the attachment. The modulus of this impedance is plotted in Figure 2, where its frequency dependence can be clearly seen.

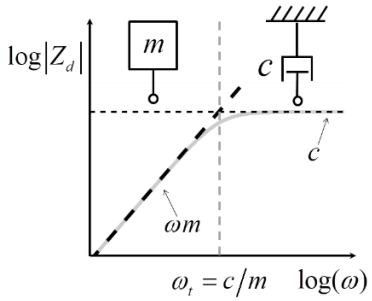

Figure 2. Mechanical impedance of a series combination of a viscous damper and a mass.

The low frequency behaviour, when $\omega << \omega_t$ in which $\omega_t = c/m$ is the transition frequency, is given by the thick dashed line, which is $|Z_d|_{\omega<<\omega_t} = \omega m$. At high frequencies when $\omega >> \omega_t$ then $|Z_d|_{\omega>>\omega_t} = c$, which is given by the thin horizontal dashed line. It is thus clear that the ratio of c/m is the quantity to be adjusted to ensure that the attachment acts as a damper and not as a mass in the frequency range of interest.

Although the problem of not having a convenient ground is solved by using a mass, as with the Lanchester damper, a further problem occurs in that a spring is required to be placed in parallel with the damper to support the mass (especially when working in the vertical direction, i.e., against gravity), resulting in potential further undesirable dynamic behaviour. The attachment now has a natural frequency of $\omega_n = \sqrt{k/m}$, where k is the spring stiffness, and this is required to be as low as possible so that the device broadly behaves as a Lanchester damper rather than a dynamic vibration absorber. To achieve this, and to maintain a low static displacement when the attachment is orientated in the vertical direction, a linear spring with high-stiffness (which supports the load with minimal deflection) is combined with a nonlinear negative stiffness element to realise the high-static and low-dynamic stiffness characteristic [37]. In principle, a quasi-zero stiffness spring would be ideal for such purposes [40], whose force-displacement characteristic is shown in Figure 3, along with a schematic of the attachment.

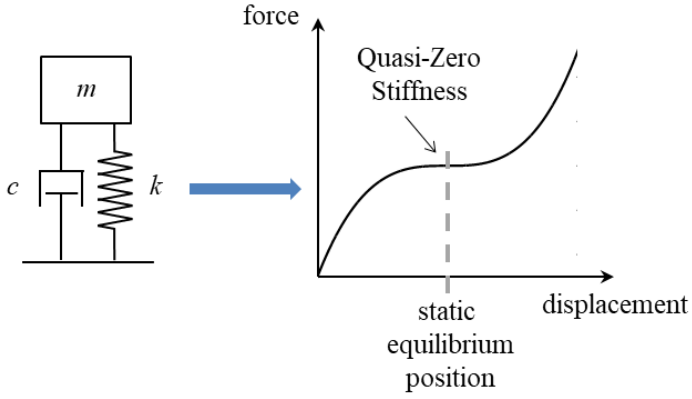

Figure 3. Design requirements for a damping attachment, in which *c/m* is much lower than the lowest natural frequency of the host structure.

3 Mechanical implementation of the device: kinematic and quasi-static analysis

The model of the proposed translational Lanchester damper with quasi-zero stiffness is illustrated in Figure 4, and it consists of a combination of a five-bar linkage with a pair of linear springs, in parallel with the viscous damper. In this device, the damping arises from the connections between the rigid links and the spring elements in the suspension device [37]. Although a complex nonlinear relation between the translational equivalent damper and its physical sources exists, the dynamic working conditions of the device are assumed to be such that both stiffness and damping are broadly linear about the static equilibrium position.

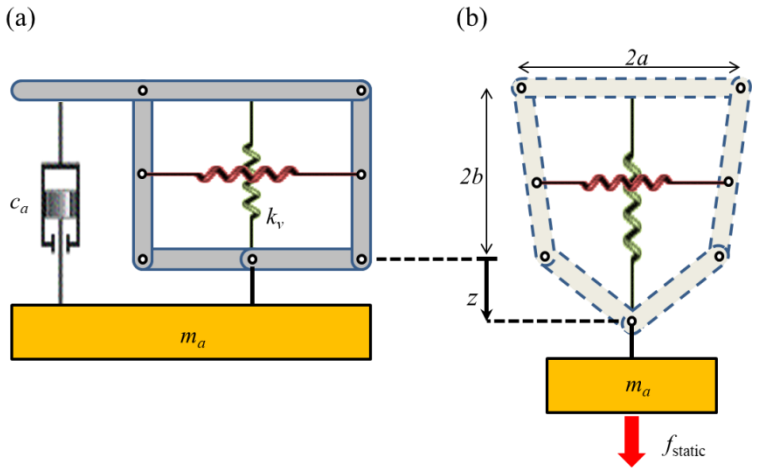

Figure 4. Mechanical implementation of the Lanchester damper with quasi-zero stiffness suspension: (a) equilibrium configuration when subject to static load due to the device mass only, and (b) linkage configuration when subject to an additional external static excitation.

Figure 4(a) shows the configuration of the device when subject only to the weight due to its mass, and Figure 4(b) shows the configuration when a static external force is also considered. The two springs only work in tension during the operation of the device. In the equilibrium configuration illustrated in Figure 4(a), the horizontal spring does not contribute to the vertical load, so the mass is only supported by the vertical spring. In the deformed configuration illustrated in Figure 4(b), the horizontal spring helps to balance the vertical external static force through the linkage configuration.

The five-bar linkage in Figure 4 has two degrees-of-freedom, but due to the symmetry of the system and the loading condition, the mechanism deforms mainly along the vertical direction [37]. A slight movement along the horizontal direction only manifests in the event of undesired asymmetric effects. The slider-crank

mechanism illustrated in Figure 5 is thus considered an appropriate model of the stiffness components of the system in Figure 4.

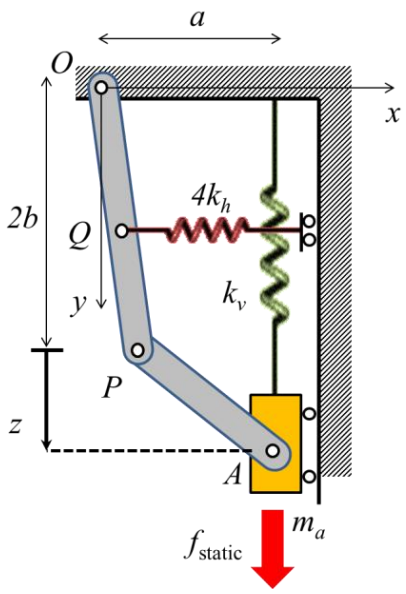

Figure 5. Slider-crank model of the device.

The external static force in Figure 5 is balanced by two elastic components acting in parallel. Since the objective is to realise a quasi-zero stiffness behaviour, and one component is due to the positive stiffness of the vertical linear spring, the other component due to the horizontal spring through the linkage should have a negative stiffness. To achieve such characteristic, the horizontal spring must be assembled with a pre-set tension, so that its free length is less than the assembled length a.

The aim of the following analysis is to better understand the nonlinear effects on the device behaviour, so that they can be avoided by a proper design strategy, and linear-like regime can be effectively exploited.

3.1. Negative stiffness component

Negative stiffness has been achieved using linear springs arranged in several geometric configurations, for example using the classical one pair of oblique springs [34], two pairs of oblique springs [41,42], or scissor-like structures [43]. In this paper, the negative stiffness is realised through a specific mechanical linkage and one linear spring only. Due to the linkage in the suspension system, it has some singular configurations [44], which are illustrated in Figure 6(a) and (b), and are determined from

$$z_{s+,s-} = -2b + 2\sqrt{b^2 \pm ab} \tag{4a,b}$$

where the subscript *s* stands for singular, + and – indicate the positive and negative sign of the displacement *z*. From Equations (4a,b), it is evident that when $b < a$, only one real singular configuration exists, as shown in Figure 6(a). Figure 6(b) shows both singular configurations of the linkage when *b* is greater than *a*.

There are two additional critical configurations in the linkage of Figure 5, which are illustrated in Figure 6(c,d) and are related to the possible collisions among the links. In Figure 6(c) the link of length *a* collides with the base, while in Figure 6(d) the link of length *a* collides with its symmetric counterpart. From the geometry of the system, the condition in Figure 6(c) occurs when $b < 2^{-1/2} a \approx 0.7a$, and the condition in Figure 6(d) occurs when $b > 2^{-1/2} a \approx 0.7a$. In terms of the displacement *z*, these two conditions occur when

$$z_{b-} = -2b, \qquad z_{l-} = -2b - a + \sqrt{4b^2 - a^2} \tag{5a,b}$$

where the subscript *b* stands for base, and *l* stands for links.

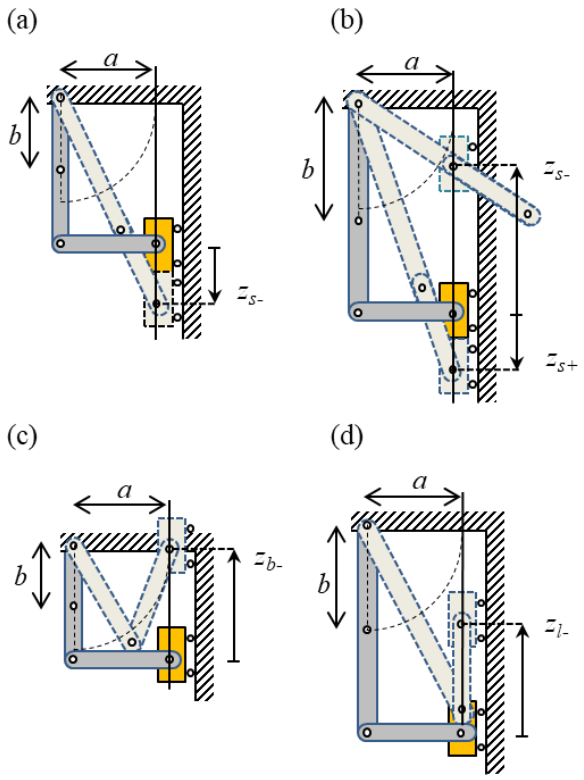

Figure 6. Geometric limits of the slider-crank linkage. Singular configurations in the case when (a) $b < a$ and (b) $b > a$; configurations denoting internal collisions in the case when (c) $b < 0.7a$ and (d) $b > 0.7a$.

The contribution to the vertical static force, as a function of the vertical displacement *z* is determined from the elastic potential energy of the horizontal spring to give

$$f_h = -4k_h\left(a - x_Q - \alpha a\right)\frac{dx_P}{dz} \tag{6}$$

where x_Q is the horizontal coordinate of point *Q* in Figure 5, and α is related to the free length of the horizontal spring $a\alpha$, which is assembled in tension so that the $\alpha < 1$. With reference to Figure 5, $x_Q = x_P/2$, where the point *P* is the intersection between a circle of radius 2*b* centred at point *O*, and a circle of radius *a* centred at point *A*. The displacement of point *P* is given by

$$x_P = \frac{a\left(8b^2 + 4bz + z^2\right) - \sqrt{\left(2b+z\right)^2\left(16a^2b^2 - z^2\left(4b+z\right)^2\right)}}{2\left(a^2 + \left(2b+z\right)^2\right)} \tag{7}$$

Substituting for x_P into Equation (6) results in

$$\begin{aligned} f_h = k_h \frac{(2b+z)}{\left(a^2+(2b+z)^2\right)^2}\left(a - \alpha a + \frac{-a\left(8b^2+4bz+z^2\right) + \sqrt{-(2b+z)^2\left(-16a^2b^2 + z^2(4b+z)^2\right)}}{4\left(a^2+(2b+z)^2\right)}\right)\cdots \\ \cdots\left(\begin{array}{l} 2\left(a\left(8b^2+4bz+z^2\right) - \sqrt{-(2b+z)^2\left(-16a^2b^2+z^2(4b+z)^2\right)}\right) - \left(a^2+(2b+z)^2\right)\cdots \\ \cdots\left(2a + \dfrac{-16a^2b^2 + z\left(32b^3+56b^2z+24bz^2+3z^3\right)}{\sqrt{-(2b+z)^2\left(-16a^2b^2+z^2(4b+z)^2\right)}}\right) \end{array}\right) \end{aligned} \tag{8}$$

Equation (8) is quite cumbersome to be of any direct use, however, it can be expanded into Taylor series to give

$$f_h = 2k_h(-1+\alpha)z + \frac{k_h(-1+2\alpha)z^3}{2a^2} + \frac{5k_h(-1+\alpha)z^4}{8a^2b} + \frac{3k_h(-1+2\alpha)z^5}{8a^4} + O[z]^6 \quad (9)$$

which is simple enough to examine the main characteristics: (i) it is not symmetric, but asymmetry only has an effect for relatively high values of displacement, since the lowest even term is of fourth-order; (ii) the asymmetry is reduced if α is increased; (iii) for small displacements, the linear stiffness does not depend on *a* and *b*, i.e. on the dimensions of the device; (iv) the dimension *b* is only important for relatively high displacements, since it first appears into the fourth-order term; (v) for relatively small values of displacement, the nonlinearity decreases with an increase in *a*, so that the longer the horizontal links, the smaller the nonlinear effect.

For subsequent use, Equation (9) is limited to the third term only and is further normalised by introducing the non-dimensional displacement $\breve{z} = z/a$, the non-dimensional force $\breve{f}_h = f_h/ak_h$ and the ratio $\breve{b} = b/a$, to yield

$$\breve{f}_h \approx 2(\alpha-1)\breve{z} + \frac{(2\alpha-1)}{2}\breve{z}^3 \quad (10)$$

which is similar to the expression of the classical three-spring quasi-zero stiffness configuration working in compression [34].

To investigate the validity of the approximation made in the derivation of Equation (10), this is plotted for different values of $\breve{b}$, in Figure 7, where it is compared with the exact expression given by Equation (8) for different values of α.

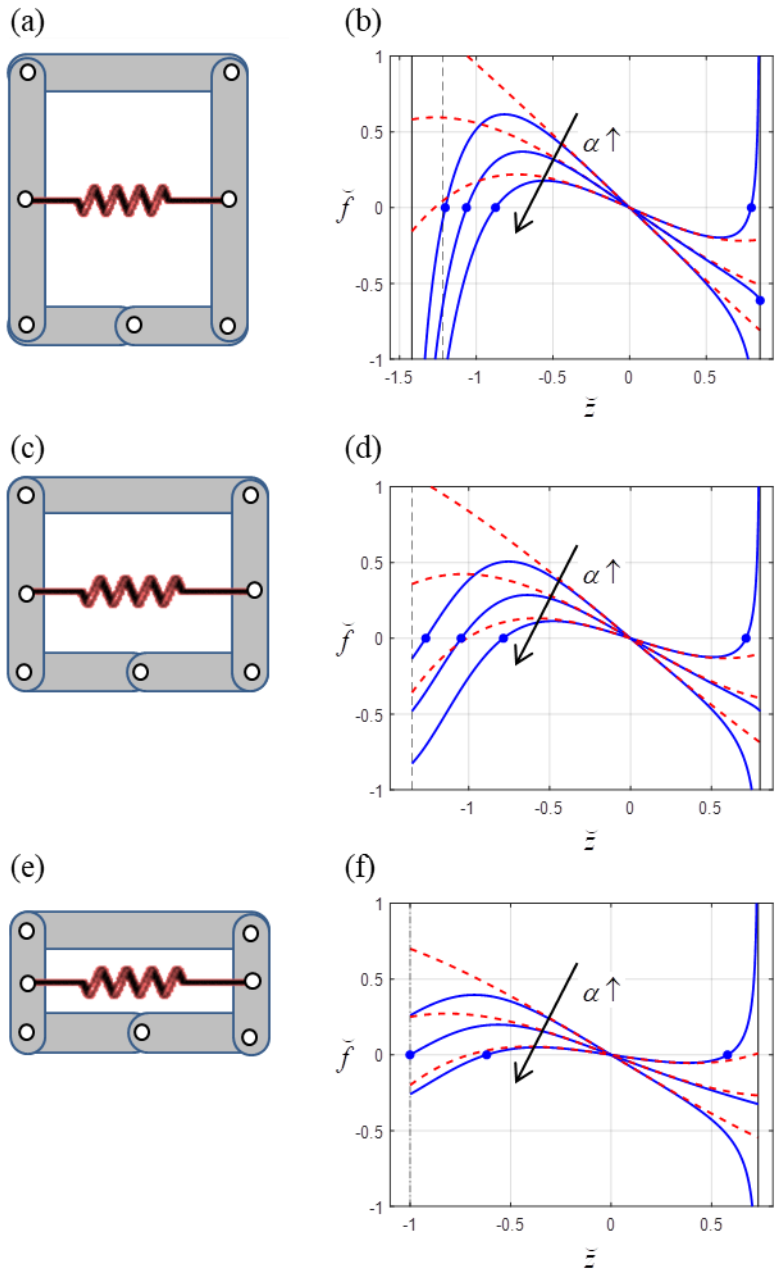

Figure 7. Negative stiffness component of the suspension for different values of the system parameters: (a,b) $\breve{b} = 1.2$ and $\alpha = 0.5177$, 0.6471, 0.7765; (c,d) $\breve{b} = 0.8$ and $\alpha = 0.5538$, 0.6923, 0.8308; (e,f) $\breve{b} = 0.5$ and $\alpha = 0.6000$, 0.7500, 0.9000. (a,c,e) Schematic of the linkage, (b,d,f) non-dimensional force-deflection curve: exact expressions (solid lines), cubic approximations (dashed lines), horizontal spring limits (circle markers), singular configuration (vertical solid lines), collision with frame (vertical dash-dotted line), collision with links (vertical dashed line).

It can be seen from Figure 7(a,b), that when $\hat{b} > 1$, the force tends to infinite values when approaching both the singular configurations given by Equations 4(a,b), which are indicated by the vertical solid lines. More specifically, when approaching the singular configuration for negative values of *z*, the force tends to $-\infty$, and

when approaching the one for positive values of *z*, the force tends to $\text{sign}(-1-\breve{b}+\alpha+2\breve{b}\alpha)\cdot\infty$, which is positive (negative) when α is greater (less) than $\alpha_{TR}=(1+\breve{b})/(1+2\breve{b})$. In Figure 7, the three values of α used to plot the curves are selected so that they are 0.8, 1 and 1.2 times the critical value α_{TR}. Note that the stiffness can be either positive or negative when approaching the asymptote for positive *z*. This is because the horizontal spring can theoretically work in tension or compression at this point, depending on its free length, which is discussed further below.

From Figure 7(c,d), when $0.7<\breve{b}<1$, there is only one singular configuration for positive values of *z*, which is indicated by the vertical solid line on the right. The dashed line on the left indicates the limit for the condition shown in Figure 6(d), given in Eq. (5b).

From Figure 7(e,f), when $\breve{b}<0.7$, the dash-dotted line on the left indicates the limit for the condition indicated in Figure 6(c), given in Eq. (5a).

Although there is a qualitative difference in behaviour given by Eq. (10) for large displacements, it is evident from Figure 7, that for displacements values less than about 40% of *a*, Equation (10) is a good approximation of Eq. (8).

3.2. Positive stiffness component and global characteristic

The vertical spring in Figure 5 supports the weight of the mass so that the device configuration at rest is such that the link of length 2*b* is vertical, and the link of length *a* is horizontal. This yields a net force $f_v=k_v z$, with the condition $2bk_v(1-\beta)=m_a g$ for equilibrium, where $2\beta b$ is the free length of the vertical spring, β is the vertical spring length factor and *g* is the acceleration due to gravity. This latter condition gives a lower limit for the stiffness k_v, which ideally should not be less than $m_a g/2b$.

To ensure quasi-zero stiffness of the device at the equilibrium configuration, the ratio of the vertical to the horizontal spring stiffness should be $\breve{k}=k_v/k_h=2(1-\alpha)$, so that the approximate non-dimensional force-displacement relationship for the whole system in Figure 5 is given by $\breve{f}_h\approx(2\alpha-1)\breve{z}^3/2$.

Other constraints may also affect the design of the suspension system. For example, readily available commercial springs usually only work in tension or compression. To ensure that the springs always work in tension in the device, the actual spring lengths are greater than their free lengths. Here, it is considered that the free length of the springs are the same as their solid lengths, to limit the number of design parameters.

For the horizontal spring, the limiting conditions correspond to $1-\breve{x}_{P\max}/2=\alpha$, where $\breve{x}_{P\max}$ is the non-dimensional maximum value of Equation (7) reached during motion. In terms of the non-dimensional displacement, this yields

$$\breve{z}_{h-}=-2\breve{b}+2\sqrt{\breve{b}^2-1+3\alpha-2\alpha^2-2\sqrt{\left(-\breve{b}^2+(-1+\alpha)^2\right)(-1+\alpha)\alpha}}$$
$$\breve{z}_{h+}=-2\breve{b}+2\sqrt{\breve{b}^2-1+3\alpha-2\alpha^2+2\sqrt{\left(-\breve{b}^2+(-1+\alpha)^2\right)(-1+\alpha)\alpha}} \qquad (11a,b)$$

where the subscript *h* stands for horizontal spring.

In the case when $\breve{b}>0.7$, the limiting condition in Figure 6(d) also applies for negative values of $\breve{z}$, so that if $\alpha<0.5$, the horizontal spring will always work in tension. However, if $\alpha>0.5$, the horizontal spring will work in tension provided that $\breve{z}>\breve{z}_{h-}$ in Eq. (11a).

In the case when $\breve{b}<0.7$, the limiting condition in Figure 6(c) also applies for negative values of $\breve{z}$, so that if $\alpha<1-\breve{b}^2$, the horizontal spring will always work in tension. However, if $\alpha>1-\breve{b}^2$, the horizontal spring will work in tension provided that $\breve{z}>\breve{z}_{h-}$ in Eq. (11a).

For positive values of $\breve{z}$, the limiting condition in Figure 6(a) applies, so that the horizontal spring will always work in tension provided that $\alpha<\alpha_{TR}$. However, if $\alpha>\alpha_{TR}$, the horizontal spring will work in tension provided that $\breve{z}<\breve{z}_{h+}$ in Eq. (11b).

For the vertical spring, the limiting condition occurs only for negative values of $\breve{z}$, as

$$\breve{z}_{v-}=-2\breve{b}\left(1-\beta\right) \qquad (11c)$$

where the subscript *v* stands for vertical spring.

The geometric limitations and spring limitations of the proposed device suspension are summarised in Appendix A, using a more detailed dimensional form.

To avoid the conditions in Equations (11a-c) both α and β should be relatively small. Combining the equations for the equilibrium of the vertical and horizontal springs results in

$$\beta = 1 - \frac{\breve{p}}{4\breve{b}\left(1-\alpha\right)} \tag{12}$$

where $\breve{p} = m_a g / a k_h$ is the non-dimensional weight of the mass, so that if α decreases, then β increases, and an accurate check is thus required. This is performed in the dynamic simulations presented in the next section.

The limits due to the horizontal free spring length are shown in Figure 7(b,d,f) by circle markers. Figure 8 then shows the global characteristic of the device suspension and corresponding limits due to both free spring lengths, for the same combinations of parameters used in Figure 7. It can be seen that as the free length of the horizontal spring increases, then the limitations due to the horizontal spring (circle markers) move towards the smaller values of $\left|\breve{z}\right|$, while the limitation due to the vertical spring ((diamond markers) moves towards the larger values of $\left|\breve{z}\right|$. Also, the value of $\breve{p}$ has to decrease for increasing values of α, to ensure that β remains positive, as indicated in Eq. (12). It can be seen that an overall linear-like quasi-zero stiffness behaviour is achieved in the approximate range where $\left|\breve{z}\right| < 0.3$, which is indicated in Figures 8(b), 8(d) and 8(f) by a shaded region.

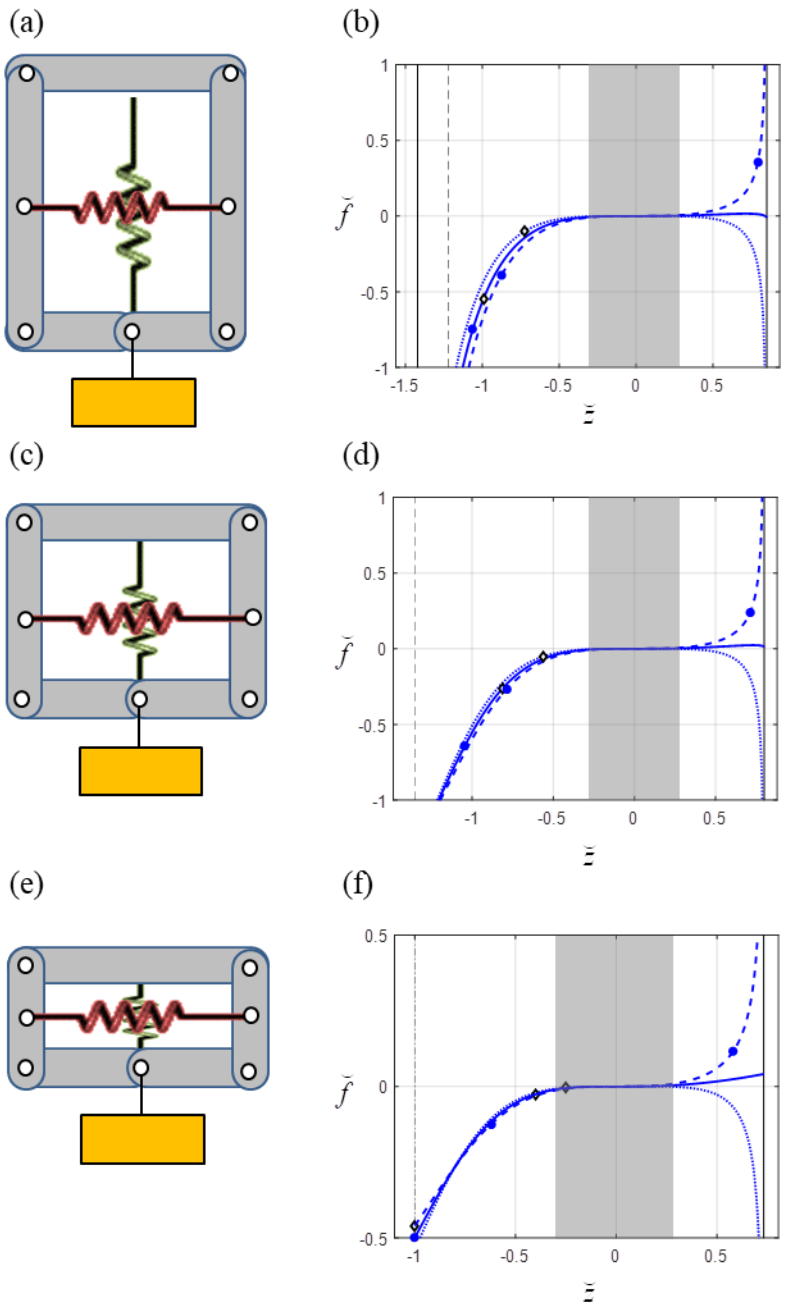

Figure 8. Global stiffness component of the suspension for different values of the system parameters: (a,b) $\breve{p} = 0.7$, $\breve{b} = 1.2$ and $\alpha =$ 0.5177, 0.6471, 0.7765; (c,d) $\breve{p} = 0.5$, $\breve{b} = 0.8$ and $\alpha =$ 0.5538, 0.6923, 0.8308; (e,f) $\breve{p} = 0.2$, $\breve{b} = 0.5$ and $\alpha =$ 0.6000, 0.7500, 0.9000. (a,c,e) Schematic of the linkage, (b,d,f) non-dimensional force-deflection curve: $\alpha = 0.8\alpha_{TR}$ (dotted lines), $\alpha = \alpha_{TR}$ (solid lines), $\alpha = 1.2\alpha_{TR}$ (dashed lines), horizontal spring limits (circle markers), vertical spring limits (diamond markers), singular configuration (vertical solid lines), collision with frame (vertical dash-dotted line), collision with links (vertical dashed line). Shaded regions in (b), (d) and (f) indicate the conditions for linear-like quasi-zero stiffness behaviour.

4 Dynamic analysis of the device: fundamental behaviour and effect of nonlinearity

In this section, the dynamic behaviour of the proposed translational Lanchester damper with quasi-zero stiffness attached to a single degree-of-freedom system host structure is investigated. The system is shown in Figure 9, where *m*, *k* and *c* are the mass, stiffness and damping of the host structure, respectively, and $f = F\cos(\omega t)$ is the excitation force. Henceforth, the symbol for the viscous linear damper in the device, illustrated in Figure 4(a), is omitted for clarity.

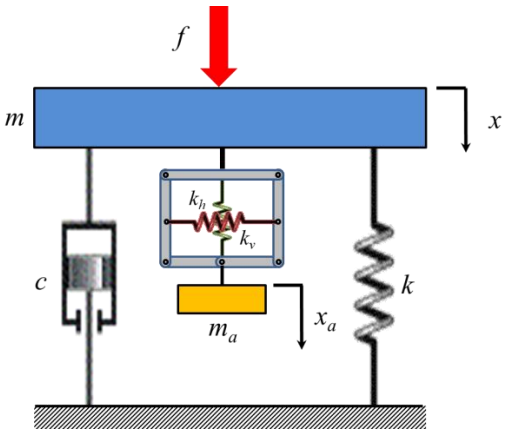

Figure 9. Lanchester damper with quasi-zero stiffness hanged from a single degree-of-freedom host structure (a viscous dashpot c_a in parallel to the vertical spring k_v is omitted for clarity).

The equations of motion of the system are

$$m\ddot{x} + c\dot{x} + kx - c_a\dot{z} - k_v z - f_h = F\cos(\omega t) \tag{13a}$$

$$m_a\ddot{x}_a + c_a\dot{z}_a + k_v z + f_h = 0 \tag{13b}$$

where f_h is given by Eq. (8), and $z = x_a - x$ is the relative displacement between the mass of the device, x_a, and the mass of the host structure, x.

To investigate the effect of the device parameters on the dynamic behaviour, Equations (13a) and (13b) are rewritten in non-dimensional form making use of the approximate expression in Equation (10), to give

$$\hat{x}''(1+\mu)+2\zeta\hat{x}'+\hat{x}=-\mu\hat{z}''+\cos(\Omega\tau) \tag{14a}$$

$$\mu\hat{z}''+2\zeta_a\hat{z}'+\gamma\hat{z}^3=-\mu\hat{x}'' \tag{14b}$$

where $\hat{x}=x/x_0$ and $\hat{z}=z/x_0$ are the non-dimensional displacement of the host structure and the non-dimensional relative displacement, respectively, with $x_0=F/k$ being the static deflection due to the static force F; $\zeta=c/2\sqrt{km}$ and $\zeta_a=c_a/2\sqrt{km}$ are the non-dimensional damping coefficients of the host structure and device, respectively; $\mu=m_a/m$ is the mass ratio; $\Omega=\omega/\omega_n$ is the non-dimensional forcing frequency, where $\omega_n=\sqrt{k/m}$; primes denote differentiation respect to the non-dimensional time $\tau=\omega_n t$, and $\gamma=(2\alpha-1)x_0^2\,k_h/2a^2k$.

4.1. Fundamental analysis of the linear zero-stiffness device

A linear analysis is performed in this section to emphasise some essential characteristics of the system behaviour. In this case, the non-dimensional equations of motion of the system are those from Eq. (14a,b) with $\gamma=0$, i.e. the Lanchester damper has zero-stiffness [35,36]. The frequency response in terms of the non-dimensional amplitude displacement $\hat{X}$ of the host structure is then given by

$$\hat{X}=\left\{\frac{\Omega^2\mu^2+4\zeta_a^2}{\Omega^2\left[4\zeta\zeta_a+\mu\left(1-\Omega^2\right)\right]^2+\left[2\zeta_a\left(1-\Omega^2\right)-2\mu\Omega^2\left(\zeta+\zeta_a\right)\right]^2}\right\}^{\frac{1}{2}} \tag{15}$$

As discussed in Section 2, if either the mass or damping of the device is very small, the device is ineffective, and if the damping is very large, then the mass of the host structure moves together with that of the device, also rendering it ineffective. An optimum damping for the linear Lanchester damper exists and was derived in [35]. This is illustrated in Figure 10, which shows the response of the host structure for different values of damping ratio. It can be noted that for relative light damping (dotted line) the peak amplitude is reduced, but the resonance frequency is not changed appreciably. When the damping is relatively high (dashed line) the

combined system behaves as a single degree-of-freedom oscillator with a mass equal to the mass of the host structure plus that of the auxiliary device. In this case, the resonant frequency shifts from 1 to $(1+\mu)^{-1/2}$. From relatively low to relatively high values of damping, the frequency response of $\hat{X}$ changes and reaches a case when the resonant peak is the lowest possible (solid line in Figure 10), which corresponds to the optimum damping value given in [35].

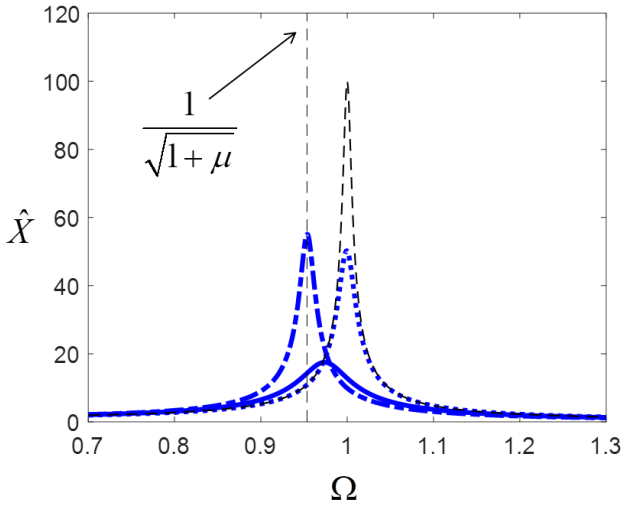

Figure 10. Effect of the non-dimensional damping on the frequency response of the system in Figure 9. Displacement amplitude of the host structure for $\mu = 0.1$, $\zeta = 0.005$, and $\zeta_a = 5$ (thick dashed line), $\zeta_a = 0.05$ (thick solid line) and $\zeta_a = 0.0005$ (thick dotted line). The frequency response of the system without the device attached is denoted by the thin dashed line.

To find a usable expression of the resonance frequency and its corresponding peak displacement amplitude, Equation (15) can be approximated in the proximity of $\Omega = 1$, for small mass ratios as

$$\hat{X} \approx \left\{ \frac{\mu^2 + 4\zeta_a^2}{\left[4\zeta\zeta_a + \mu\left(1-\Omega^2\right)\right]^2 + \left[2\zeta_a\left(1-\Omega^2\right) - 2\mu\left(\zeta+\zeta_a\right)\right]^2} \right\}^{\frac{1}{2}} \tag{16}$$

and solved for the peak to give

$$\Omega^* \approx \left[1-\frac{4\mu\zeta_a^2}{\mu^2+4\zeta_a^2}\right]^{\frac{1}{2}}, \qquad \hat{X}^* \approx \frac{\mu^2+4\zeta_a^2}{8\zeta_a^2\zeta+2\mu^2\left(\zeta_a+\zeta\right)} \tag{17a,b}$$

To calculate the minimum value of the peak, the derivative of Equation (16b) respect to ζ_a is set to zero, and solved to give $2\zeta_a = \mu$, which agrees with the optimum damping of a Lanchester damper for small values of the mass ratio [3,35,36,45]. The corresponding resonance frequency and corresponding expression for the peak are given by

$$\Omega^*_{\text{min}} \approx \sqrt{1-\frac{\mu}{2}}, \qquad \hat{X}^*_{\text{min}} \approx \frac{2}{\mu+4\zeta} \tag{18a,b}$$

To investigate the shift in the resonance frequency with respect to the original structure (without the device), Equation (18a) can be expanded in series to the first term for small values of the mass ratio to yield $\Omega^*_{\text{min}} \approx 1-\mu/4+O\left[\mu\right]^2$. Note that the shift in the resonance frequency is a function of the mass ratio only, whilst the minimum peak is a function of both the mass ratio and the damping.

4.2. Dynamic analysis of the quasi-zero stiffness device

The dynamic performance of the proposed translational Lanchester damper which exploits a quasi-zero stiffness suspension is presented in terms of the analytical frequency response curve. Although linear-like behaviour is sought for the device, the effect of the nonlinearity is investigated here to understand the limits for such a linear behaviour to be deliberately exploited.

Thus, assuming a predominantly harmonic response, Equations (14a,b) can be solved analytically by applying the harmonic balance method, and the stability of the solution studied by applying Floquet theory as detailed in [46]. Following this procedure, the amplitude-frequency equations are given by

$$a_0 + a_2\hat{Z}^2 + a_4\hat{Z}^4 + a_6\hat{Z}^6 = 0 \tag{19a}$$

$$b_2\hat{Z}^2 + b_4\hat{Z}^4 + c_2\hat{X}^2 = 1 \tag{19b}$$

where

$$a_0 = -\frac{\Omega^4}{c_2}, \quad a_2 = \Omega^4 + \left(\frac{\sigma_a}{\mu}\Omega\right)^2 + \Omega^4\frac{b_2}{c_2}, \quad a_4 = -\frac{3}{2}\frac{\gamma}{\mu}\Omega^2 + \Omega^4\frac{b_4}{c_2}, a_6 = \frac{9}{16}\left(\frac{\gamma}{\mu}\right)^2 \tag{20a-d}$$

$$b_2 = \Omega^4\mu^2 + 2\mu\Omega^2\left[1-(1+\mu)\Omega^2\right] + 2\sigma\sigma_a\Omega^2, \quad b_4 = -\frac{3}{2}\gamma\left[1-(1+\mu)\Omega^2\right] \tag{20e,f}$$

$$c_2 = \left[1-(1+\mu)\Omega^2\right]^2 + \sigma^2\Omega^2 \tag{20g}$$

Equations (19a,b) are solved for some combinations of the system parameters so that the frequency response curve of the combined two degree-of-freedom nonlinear system can be compared to that of the linear system. Using the approximate optimum damping for the ideal Lanchester damper, i.e. $2\zeta_a = \mu$, the behaviour of the system is shown in Figure 11(a,b) for a relatively low and high value of nonlinearity, respectively. For validation, the solution obtained by the numerical integration of the exact equations of motion to a stepped sine excitation is superimposed as a thick black dotted line to the approximate analytical solution of the amplitude-frequency equation. It can be seen in Figure 11(a) that the Lanchester damper with quasi-zero stiffness behaves similarly to the ideal Lanchester damper for relatively small values of nonlinearity. A relatively high increase in the nonlinearity, as Figure 11(b), is detrimental in terms of damping performance.

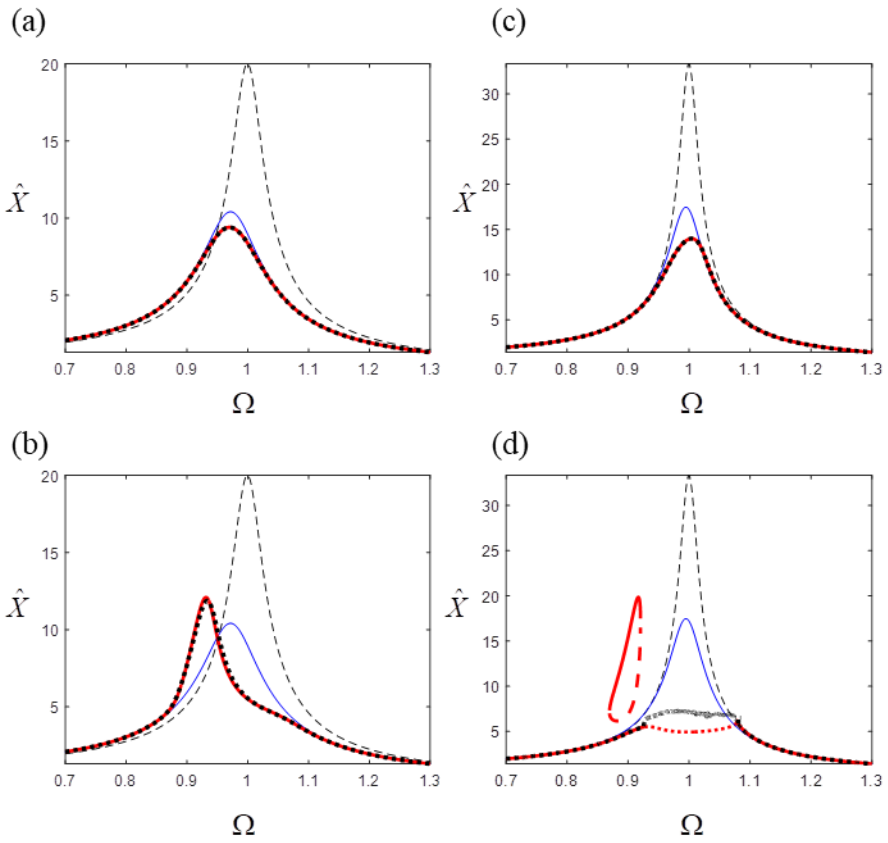

Figure 11. Effect of the device on the frequency response of the host structure. Non-dimensional displacement amplitude for (a,b) $\mu = 2\zeta_a = 0.1$, $\zeta = 0.025$ and (c,d) $\mu = 0.1$, $\zeta_a = \zeta = 0.015$. (a) $\gamma = 5\times10^{-4}$, (b) $\gamma = 45\times10^{-4}$, (c) $\gamma = 10^{-4}$, (d) $\gamma = 7\times10^{-4}$. Response with the device not attached (thin dashed line), with ideal linear device (thin solid line), and with nonlinear device: stable solutions (thick solid lines), unstable solutions (thick dashed lines), quasi-periodic solutions (thick dotted lines). Solution of the equations of motion due to a stepped sine (thicker dotted line).

If the approximate optimum damping condition is discarded, and $2\zeta_a$ is less than μ, then different dynamics can appear, as illustrated in the frequency responses shown in Figure 11(c,d). In particular, the behaviour shown in Figure11(c) is similar to that in Figure 11(a). However, when the nonlinearity is increased, as in Figure 11(d), the appearance of regions of unstable harmonic solutions (dotted line), with quasi-periodic motion [24], and detached response [25], manifest, leading to undesirable dynamics . It is worth noting that classical sweep or stepped sine excitation may not excite a detached resonance curve [46]. Quasi-periodic motion and detached curves are seen here as undesirable effects arising from pushing the device beyond its operational range in which the device has linear-like behaviour, and are not investigated further. The interested reader is directed to [24,25] for insight into the nonlinear dynamics of this type of system.

In the case where $2\zeta_a$ is greater than μ, there is no particular benefit, unless there are relatively high values of nonlinearity. Since such working condition is not the focus of the paper, it is not shown in the figures.

Provided that undesirable dynamics are thus avoided through an appropriate design, the proposed translational Lanchester damper with quasi-zero stiffness broadly performs as the ideal zero-stiffness Lanchester damper. It provides a very low stiffness in a limited displacement range around the equilibrium position, exhibiting linear-like behaviour.

4.3. Virtual experiments

To bridge the gap between a simplified analytical model and experimental work on a prototype device, some multi-body simulations were carried out. The main advantage of such simulations, with respect to the numerical solution of the equations of motion, is that physical parameters can be used, and quantitative results are accompanied by visual animations for a closer examination of the mechanical behaviour. A virtual model of the device attached to the host structure was assembled as shown in Figure 12(a), and the system response was determined in terms of a quasi-static test and a slow dynamic sweep test.

The dimensional system parameters are given in Table 1, and the result of a simulated quasi-static test is shown in Figure 12(b), together with the result from the analytical model. Animation 1, in the supplementary material, shows the simulated quasi-static test.

For the dynamic test, simulation was performed for a value of the excitation force amplitude, namely F = 0.2548 N, which corresponds to the non-dimensional parameters used in Figures 11(a). Figure 12(c) then shows the response to a slow sweep together with the results from the analytical model. The peak amplitude of the non-dimensional relative displacement resulted to be about $0.25<0.3$, which is within the limit assumed above in Section 3.2 for a linear-like behaviour. Animations 2, provided as supplementary material, show the simulated dynamic test.

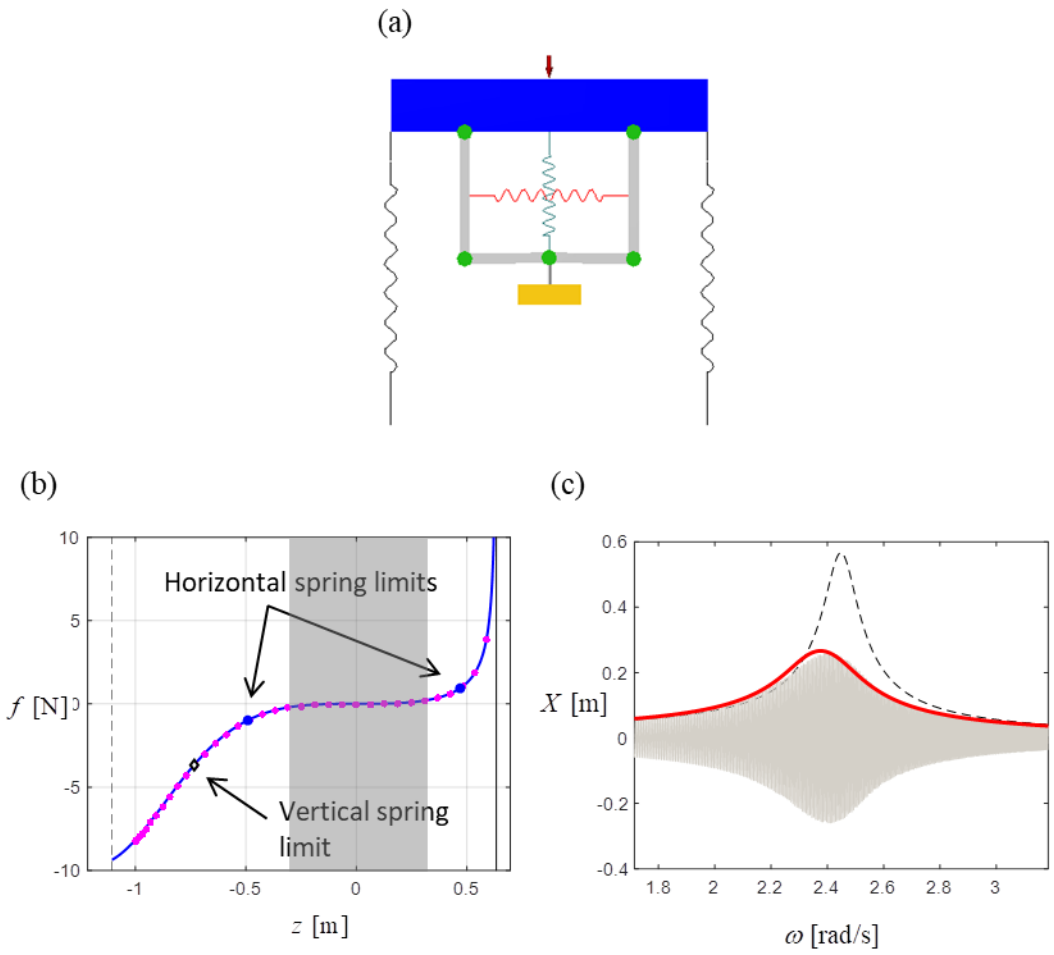

Figure 12. (a) Virtual model of the device on a single degree-of-freedom host structure with parameters in Table 1. (b) Results of a quasi-static test: multi-body (dotted line), analytical (solid line), technological springs limits (markers). (c) Dynamic results of a slow sweep test, with F = 0.2548 N: virtual experiment (thin grey line), analytical expression (thick solid line), system without device attached (dashed line). Shaded region in (b) indicates the conditions for linear-like quasi-zero stiffness behaviour.

Table 1. Parameters for the virtual experiment using multi-body simulation.

m [kg]	k [N/m]	c [Ns/m]	m_a [kg]	k_h [m]	c_a [Ns/m]	α [m]	a [m]	b [m]	g [m/s^2]
1.5	9	0.1837	0.15	10	0.3674	0.9	0.8	0.6	9.81

5 Experimental work

A prototype of the translational Lanchester damper with quasi-zero stiffness is illustrated in Figure 13(a). The linkage was designed such that a=b=0.035 m. The stiffness of the horizontal and vertical springs were

estimated from separate measurements to be k_h=2210 N/m and k_v=718 N/m, respectively, and the suspended mass was m_a=1.5 kg.

The experimental force-displacement curve was first measured by a quasi-static test, where the device was mounted in a load testing machine (ZwickiLine TH 2.5 kN), and an expanding saw tooth displacement cycle was imposed with a loading rate of 100 mm/min. The result of this test is shown in Figure 13(b) as a thick solid black line giving the hysteresis curve. Also shown in the graph are the predicted exact and approximate force-displacement curves as thin solid and dashed lines respectively, and the theoretical limits due to the free lengths of the springs. The equivalent free spring length factors of the horizontal and vertical springs were estimated based on the expressions reported in Section 3.2 to be $\beta = 1 - m_a g / 2bk_v = 0.7072$ and $\alpha = 1 - k_v / 2k_h = 0.8376$. Examining Figure 13(b), it can be seen that the experimental test was performed up the technological limit of the vertical spring. The non-dimensional condition assumed in Section 3.2 for linear-like behaviour, now reflects in about $|z| < 0.01$ m, which is indicated by the shaded region in Figure 13(b).

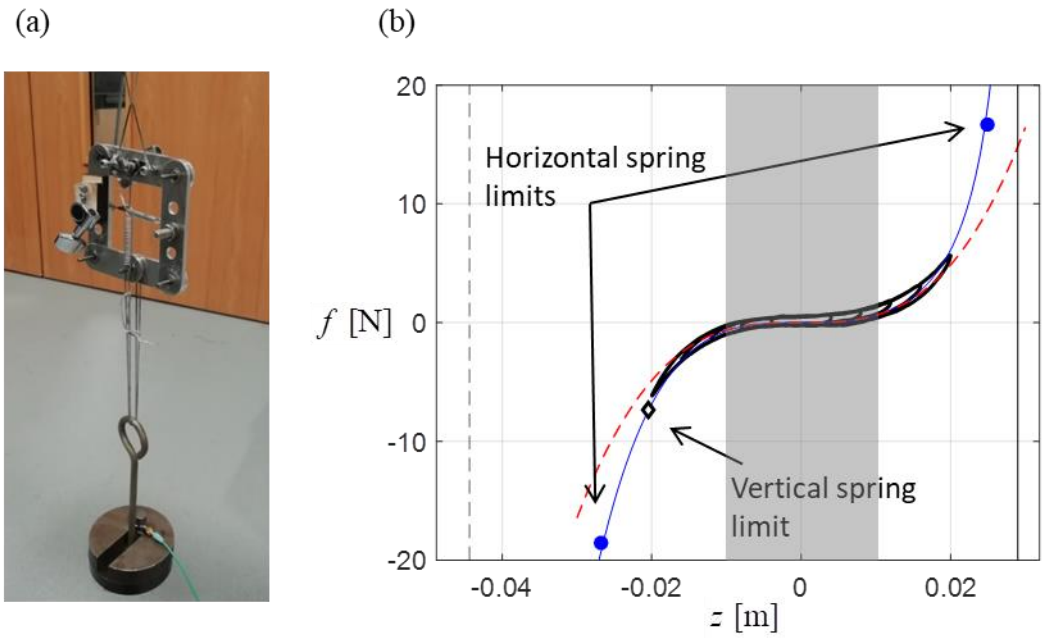

Figure 13. Physical prototype of the device. (a) Photograph of the device with suspended mass in its equilibrium configuration. (b) Result of an experimental quasi-static test: hysteretic cycle (thick solid line), theoretical curve (thin solid line), cubic approximation (thin dashed line), spring free length limits (markers). Shaded region in (b) indicates the conditions for linear-like quasi-zero stiffness behaviour.

5.1. Attachment of the device to a simple oscillator

The prototype device was mounted on a long-stroke vibration shaker (APS113 ELECTRO-SEIS®), which emulates a forced single degree-of-freedom oscillator, as shown in Figure 14. The shaker moving mass with support features attached was 6.8 kg, and the mass of the device was 2.2 kg in this case. The stiffness and damping of the shaker were then estimated by linear fitting, as 2400 N/m and 22.72 N/ms^2, respectively. The horizontal and vertical spring of the device were manually adjusted until the device was approximately in its quasi-zero stiffness condition, and the damping was estimated, assuming linear-like behaviour, to be 11.61 N/ms^2.

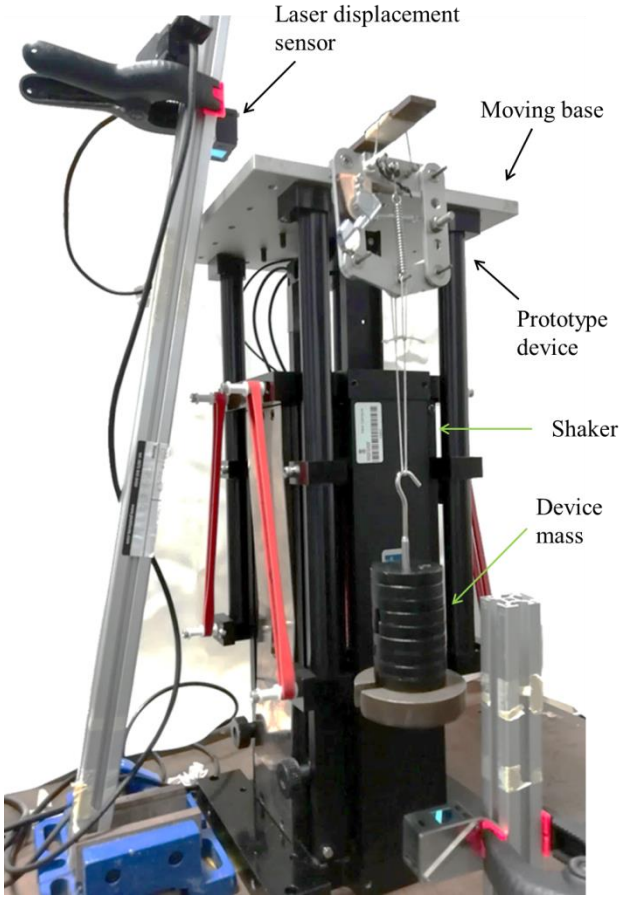

Figure 14. Photograph of the prototype device mounted on an electro-dynamic shaker, which emulated a force single degree-of-freedom oscillator.

Experimental data were collected at single excitation frequencies and low excitation amplitude to induce linear-like behaviour. A reference voltage supplied to the shaker amplifier was measured as was the displacement of the shaker mass using a displacement laser sensor (Omron ZX2-LD100). Three experiments were conducted. In the first test, the frequency response between the reference voltage and the shaker displacement of the shaker alone (device removed) was measured. In the second test, the mass of the device was directly connected to the shaker, and the same frequency response was measured again. In the third test, the effect of the device on the

shaker was measured, again using the same frequency response. Figure 15 shows the experimental measurements (dynamic displacement/displacement at 1 Hz) along with the corresponding linear fitted model.

It is first noted that the results in Figure 15 are similar to those in Figure 10. In particular, it can be seen that the effect of the device (solid line and circles) is to introduce additional damping to the shaker. At low frequencies (around 2 Hz), however, locking of the device linkage occurred due to friction in the bearings, and this is evident from the experimental data (circles). In this region, the shaker and the device moved together, and the experimental data thus follows the dash-dotted line. When the frequency was high enough to break the internal friction in the linkage, then the experimental data shift, and align to the frequency response of the shaker alone with a resonance at about 3 Hz, as expected from the discussion in Section 4. A simple linear viscous damping model (thick solid line in Figure 15) is thus assumed to represent the experimental system dynamics (circles) once friction-locking has been broken. The assumption of such linear-like behaviour for damping is based on the relative small displacement amplitude across the device, which did not exceed the threshold of 0.01 m highlighted in Figure 13(b).

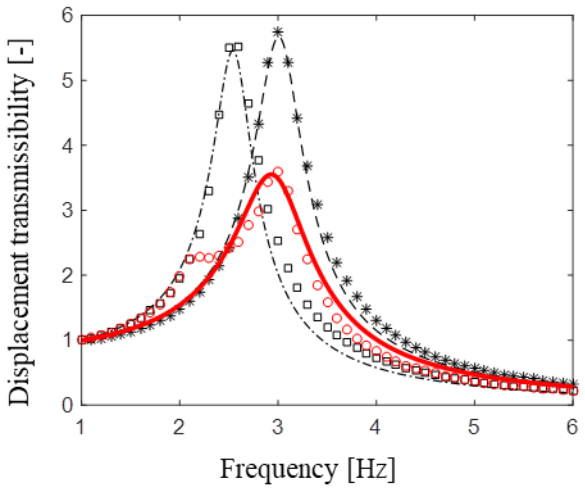

Figure 15. Results of the experimental test with the device on an electro-dynamic shaker. Displacement transmissibility of the shaker alone: experiments (asterisks), and model (thin dashed line). Displacement transmissibility of the shaker plus the mass of the device: experiments (squares), and model (thin dash-dotted line). Displacement transmissibility of the shaker with attached device: experiments (circles), and model (thick solid line).

5.2. Attachment of the device to multi-modal structures

The device was attached to two different multi-modal structures. The aim of these tests was to demonstrate the efficacy of the device on real engineering structures. The device was first attached to the tip of a cantilever steel beam with cross-sectional dimensions 100 mm × 50 mm, wall thickness 3 mm, with a free length of 1.8 m

(estimated weight about 13 kg), as shown in Figure 16(a). Excitation was provided by a shaker (Dataphysics Signal Force V20) hanging from a supporting structure, using a stinger and a force transducer (PCB 208C03) located at approximately 0.7 m from the fixed end. An accelerometer (PCB 352C03) was located on the beam tip where the device was attached. A vibration controller and data acquisition system (Dataphysics Abaqus 730) was adopted, and a swept sine signal was used to excite the beam over a range of 5–600 Hz with a logarithmic sweep lasting 40 s. The device mass was 1.5 kg. The measured frequency response of the beam with and without the device is shown in Figure 16(b) as a solid and dashed line, respectively. For a better overall visualization, the accelerance is plotted, and a logarithmic scale is adopted. A detailed analysis of the effectiveness of the device is given following the description of the second multi-modal structure experiment.

(a)

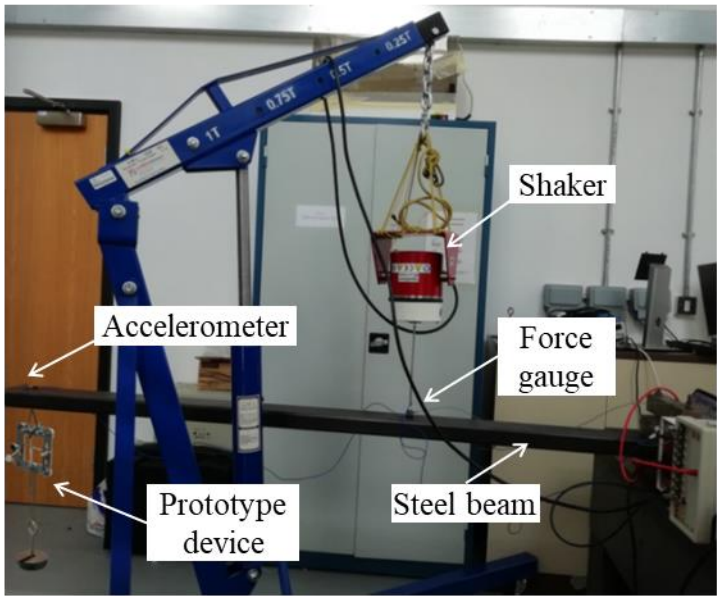

(b)

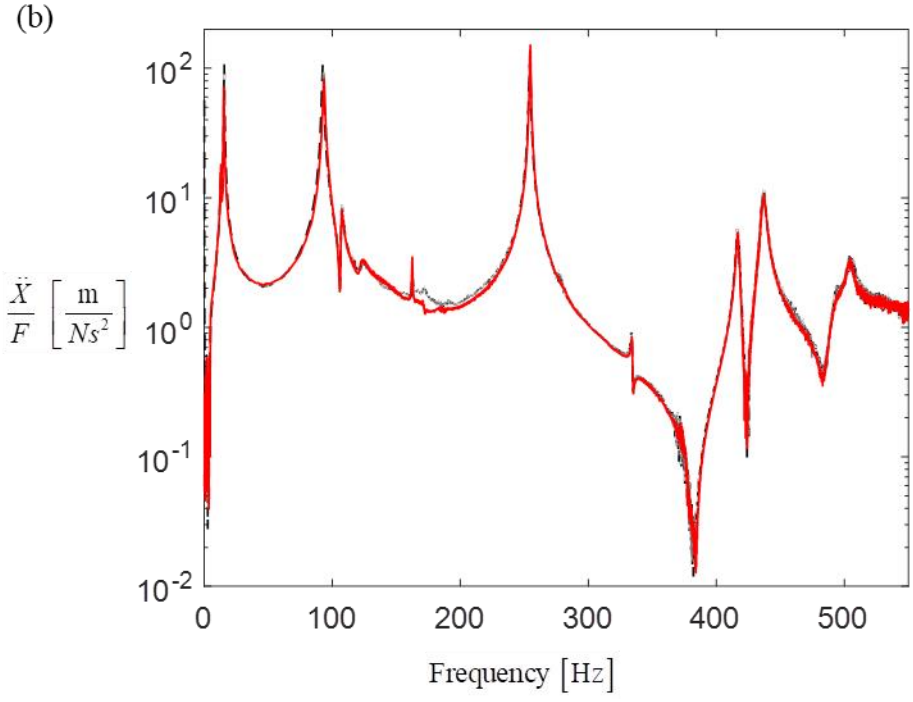

Figure 16. Experimental setup of the device connected to a cantilever beam. (a) Photograph and (b) frequency response without (dashed line) and with the device attached (solid line).

The device was then attached to the tip of a wind turbine blade constructed from glass reinforced plastic, with a free length of approximately 2.3 m and mass approximately 11 kg, as shown in Figure 17(a), but in this case, the device mass was 1 kg. The measured frequency response of the blade with and without the device is shown in Figure 17(b) as a solid and dashed line, respectively. Again, for better overall visualization, the accelerance is plotted, and a logarithmic scale is adopted. Excitation was provided by a shaker (Dataphysics Signal Force V20) hanging from a supporting structure, using a stinger and a force transducer (PCB 208C03) located at approximately 0.2 m from the fixed end. An accelerometer (PCB 352C03) was located on the tip of the blade where the device was attached. A vibration controller and data acquisition system (Dataphysics Abaqus 730) was adopted, and a swept sine signal was used to excite the blade over a range of 5–100 Hz with a logarithmic sweep lasting 40 s.

For both experiments, it was verified that the displacement amplitude across the device did not exceed the limit of 0.01 m highlighted in Figure 13(b) as the threshold for the linear-like behaviour.

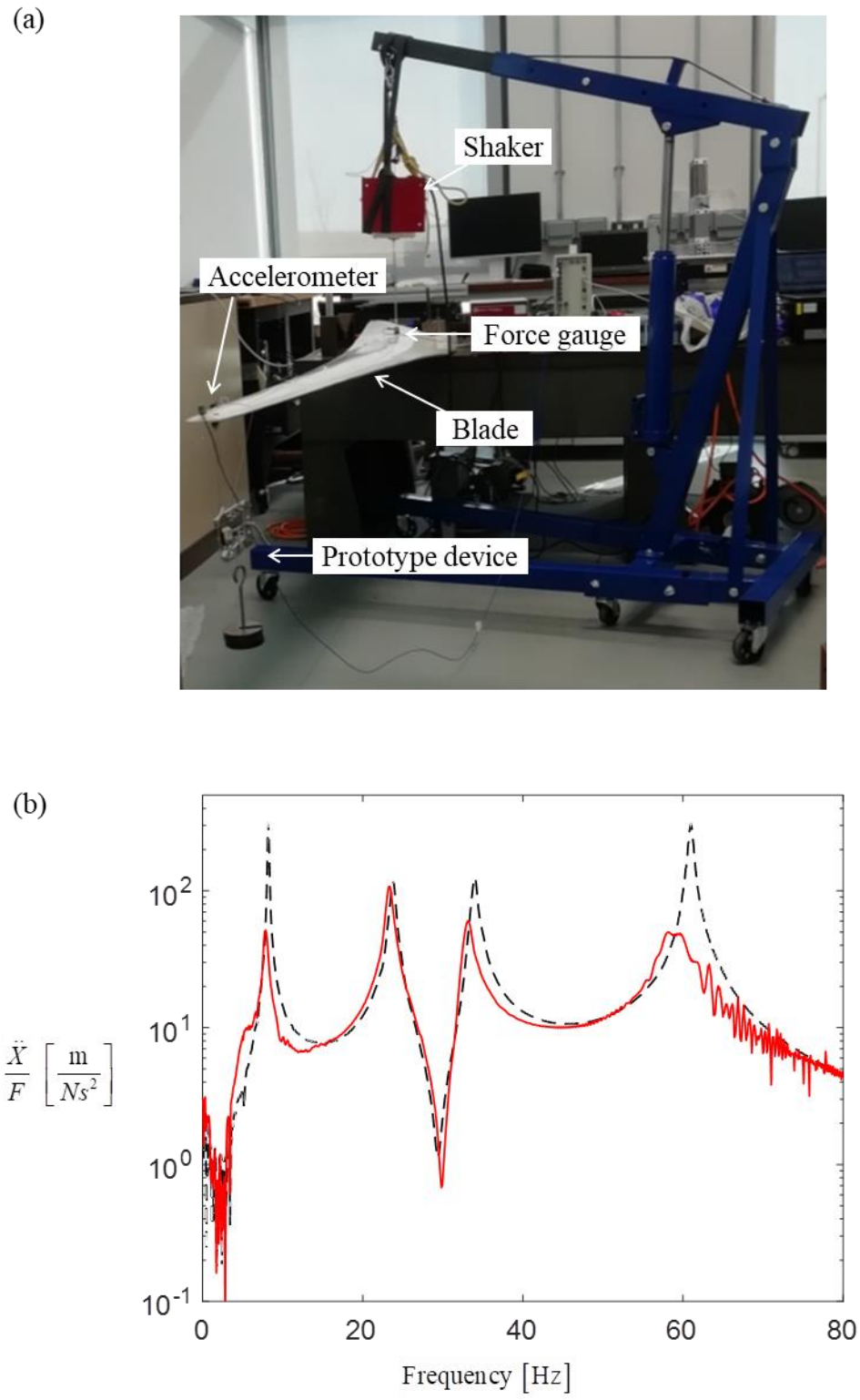

Figure 17. Experimental setup of a wind turbine blade. (a) Photograph and (b) frequency response without (dashed line) and with the device attached (solid line).

From a preliminary observation, it can be seen that the effect of the device is much more evident on the blade than on the beam. However, for better insight, a close-up of both frequency response curves close to the first natural frequency in each case are shown in Figure 18(a) and (b), for the beam and the blade, respectively. Now,

rather than accelerance, the receptance is plotted using a linear scale, so that the results can be compared to the theoretical predictions based on Section 4. Along with the results of the structures with and without the device attached, the frequency response of the structure with the device mass directly attached to the host structures via a Dyneema® cord are also shown as dash-dotted lines. The purpose of this latter measurement is to facilitate a better comparison between the theoretical and experimental results.

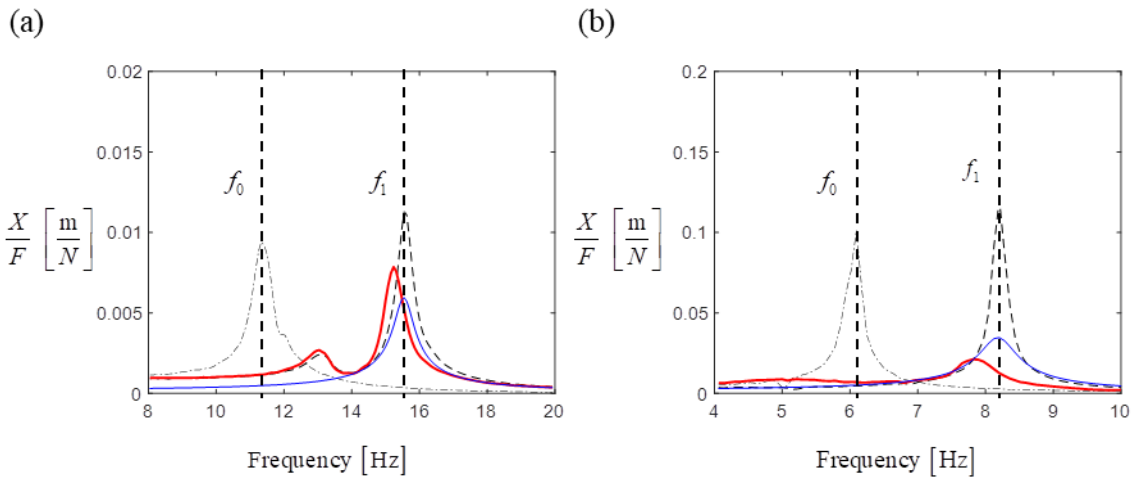

Figure 18. Close-up of the measured frequency response around the first mode of (a) the beam and (b) the blade: structure alone (thin dashed line), with device mass directly attached (thin dash-dotted line), with the device on (thick solid line). Theoretical expectation using a linear ideal zero-stiffness device is indicated with a thin solid line.

Figures 18(a) and (b) again illustrate the effect shown earlier in Figure 10. By denoting the first resonance frequency of the structure alone as f_1 and the first natural frequency of the host structure with directly attached device mass m_a, as f_0 , it is possible to estimate an equivalent single degree-of-freedom model of the structure by the following system of equations

$$(2\pi f_1)^2 = \frac{k_{eq}}{m_{eq}}, \qquad (2\pi f_0)^2 = \frac{k_{eq}}{m_{eq} + m_a} \tag{21a,b}$$

where k_{eq} and m_{eq} are the unknown equivalent stiffness and mass of the structure, in the single degree-of-freedom assumption. The solutions for k_{eq} and m_{eq} are given in Table 2. The damping estimates using the half-power points are also given in Table 2, as is the mass ratio μ_{eq} between the device mass and m_{eq}, and the mass ratio μ_{eff} , between the device mass and the mass of the structure. Also shown in Table 2 is the load factor λ, which is a simple scaling factor adopted to account for the fact that the excitation force on both structures was not collocated with the device.

Equation (15) in Section 4.1 is used to estimate the value of damping ζ_a in the device, assuming that it is a linear zero-stiffness device. Since the device suspension was the same on both structures, a trade-off estimate of

the damping coefficient resulted in c_a = 3 Ns/m, which leads to ζ_a = 0.009 for the beam experiment and ζ_a = 0.024 for the blade experiment. The theoretical result is plotted as thin solid lines in Figure 18(a) and (b). It can be seen that although very crude estimates and assumptions have been made, the theoretical expectations fundamentally captured the measured experimental behaviour.

Table 2. Estimated parameters of the equivalent single degree-of-freedom model of the experimental structures in their first mode of vibration.

	f_0 [Hz]	f_1 [Hz]	m_{eq} [kg]	k_{eq} [N/m]	ζ [-]	μ_{eq} [-]	μ_{eff} [-]	λ [-]
Beam	11.33	15.55	1.70	1.62×10^4	0.01	0.88	0.11	3.68
Blade	8.20	6.09	1.23	3.27×10^3	0.0095	0.81	0.09	7.51

It should be noted that no attempt was made to optimise the damping in the prototype device, as the research focussed on the stiffness element. On the other hand, the optimal damping is dependent upon the structure to which the device is attached and various articles, e.g. [3,35,36,45], have reported this since the invention of the original damper by Lanchester.

6 Conclusions

This paper has presented an investigation into the design of a quasi-zero stiffness element used in parallel with a translational Lanchester damper. This device has the advantage of being inertial and capable of adding damping to a structure over a broad range of frequencies, unlike the dynamic vibration absorber, which is tuned to a specific frequency. The key is to design the spring element in the device so that its stiffness is close to zero. To achieve this, a nonlinear negative stiffness was used in this paper, which was realised using a combination of a linear spring and few rigid links arranged in a specific configuration. Essentially, the negative stiffness was exploited in parallel to the linear stiffness element to obtain the global quasi-zero stiffness effect. The working condition of the device was designed to limit undesired nonlinear behaviour during dynamic motion, and this restricted the displacement amplitude across the linkage. The design constraints and how they affect the nonlinearity have been investigated, resulting in general guidelines to achieve a desired linear-like behaviour of the device during operation. A prototype of the device was manufactured and tested on a single mode and two multi-modal structures to validate the theory, demonstrating the efficacy of the device.

Funding: A.D. Shaw and M.J. Brennan would like to acknowledge financial support from the Royal Academy of Engineering [Grant No. DVF1617\6\3].

Declarations of interest: none.

Appendix A. Limitations due to geometry and springs for the proposed device

	Geometric limits				Spring limits			
	Singular configuration ($z > 0$)	Singular configuration ($z < 0$)	Collision to frame ($z < 0$)	Collision between links ($z < 0$)	Horizontal spring limit ($z < 0$)	Horizontal spring limit ($z > 0$)		Vertical spring limit ($z < 0$)
	$\tilde{z}_{s+}$	$\tilde{z}_{s-}$	$\tilde{z}_{b-}$	$\tilde{z}_{l-}$	$\tilde{z}_{h-}$	$\tilde{z}_{h+}$		$\tilde{z}_{v-}$
$\frac{b}{a} > 1$	$-2b+2\sqrt{b^2+ab}$	$-2b+2\sqrt{b^2-ab}$	-	$-2b-a+\sqrt{4b^2-a^2}$	$\alpha < 0.5$	$\alpha < \frac{b+a}{2b+a}$	-	$-2\frac{b}{a}(1-\beta)$
$0.7 \le \frac{b}{a} \le 1$					$\alpha \ge 0.5$		(*)	
$\frac{b}{a} < 0.7$		-	$-2b$	-	$\alpha < 1-\frac{b^2}{a^2}$	$\alpha \ge \frac{b+a}{2b+a}$	(**)	
					$\alpha \ge 1-\frac{b^2}{a^2}$		(*)	
Schematics	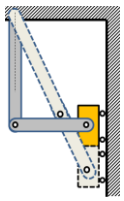	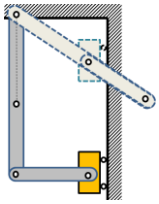	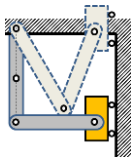	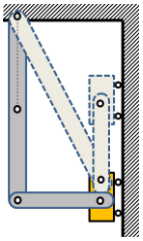	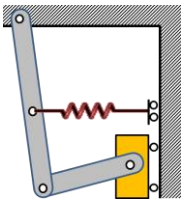	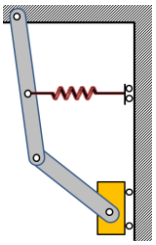		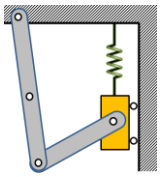

(*) $-2b+2\sqrt{b^2-2\sqrt{a^2\left(-b^2+a^2(-1+\alpha)^2\right)(-1+\alpha)\alpha}+a^2\left(-1+3\alpha-2\alpha^2\right)}$

(**) $-2b+2\sqrt{b^2+2\sqrt{a^2\left(-b^2+a^2(-1+\alpha)^2\right)(-1+\alpha)\alpha}+a^2\left(-1+3\alpha-2\alpha^2\right)}$

References

[1] F.W. Lanchester, Damping torsional vibrations in crank shafts, U.S. Patent No. 1085443 (1914).

[2] E.S. Taylor, Eliminating crankshaft torsional vibration in radial aircraft engines, SAE Technical Papers 1936. https://doi.org/10.4271/360105

[3] Y.H.J. Au, K.W. Ng, R.W. New, Lanchester damper - a design procedure for optimizing the damping ratio for a cylindrical slug damper fitted to a machine element, Journal of Mechanical Design Transaction of the ASME 101 (1979) 291-297. https://doi.org/10.1115/1.3454051

[4] J. Ormondroyd, J.P. Den Hartog, The theory of the dynamic vibration absorber, ASME Journal of Applied Mechanics 50 (1928) 9-22.

[5] J.P. Den Hartog, Mechanical Vibrations, McGraw-Hill, New York, 1956.

[6] D.J. Mead. Passive vibration control, John Wiley & Sons, 1st edition, 1999.

[7] T. Detroux, G. Habib, L. Masset, G. Kerschen, Performance, robustness and sensitivity analysis of the nonlinear tuned vibration absorber, Mechanical Systems and Signal Processing 60–61 (2015) 799-809. https://doi.org/10.1016/j.ymssp.2015.01.035

[8] N.A. Alexander, F. Schilder, Exploring the performance of a nonlinear tuned mass damper, Journal of Sound and Vibration, 319 (2009) 445-462. https://doi.org/10.1016/j.jsv.2008.05.018

[9] G. Gatti, Fundamental insight on the performance of a nonlinear tuned mass damper, Meccanica 53 (2018) 111-123. https://doi.org/10.1007/s11012-017-0723-0

[10] G. Habib, T. Detroux, R. Viguie, G. Kerschen, Nonlinear generalization of Den Hartog's equal-peak method, Mechanical Systems and Signal Processing 52–53 (2015) 17-28. https://doi.org/10.1016/j.ymssp.2014.08.009

[11] M.J. Brennan, G. Gatti, The characteristics of a nonlinear vibration neutralizer, Journal of Sound and Vibration 331 (2012) 3158-3171. https://doi.org/10.1016/j.jsv.2012.02.010

[12] B. Tang, M.J. Brennan, G. Gatti, N.S. Ferguson, Experimental characterization of a nonlinear vibration absorber using free vibration, Journal of Sound and Vibration 367 (2016) 159-169. https://doi.org/10.1016/j.jsv.2015.12.040

[13] M. Febbo, S.P. Machado, Nonlinear dynamic vibration absorbers with a saturation, Journal of Sound and Vibration 332 (2013) 1465-1483. https://doi.org/10.1016/j.jsv.2012.11.025

[14] A. Elías-Zúñiga, L.M. Palacios-Pineda, D. Olvera-Trejo, O. Martínez-Romero, Broadening the frequency bandwidth of a finite extensibility nonlinear vibration absorber by exploiting its internal resonances, Nonlinear Dynamics 102 (2020) 1239-1270. https://doi.org/10.1007/s11071-020-05721-4

[15] W.R.A. Godoy, M.A. Trindade, Design and analysis of a geometrically nonlinear dynamic vibration absorber, Journal of Computational and Nonlinear Dynamics 15 (2020) 081002. https://doi.org/10.1115/1.4047335

[16] D. Zou, G. Liu, Z. Rao, T. Tan, W. Zhang, W.H. Liao, A device capable of customizing nonlinear forces for vibration energy harvesting, vibration isolation, and nonlinear energy sink, Mechanical Systems and Signal Processing 147 (2021) 107101. https://doi.org/10.1016/j.ymssp.2020.107101

[17] O.V. Gendelman, Transition of Energy to a Nonlinear Localized Mode in a Highly Asymmetric System of Two Oscillators, Nonlinear Dynamics 25 (2001) 237-253. https://doi.org/10.1023/A:1012967003477

[18] O.V. Gendelman, A.F. Vakakis, Energy pumping in nonlinear mechanical oscillators: Part II – Resonance capture, Journal of Applied Mechanics Transactions ASME 68 (2001) 42-48. https://doi.org/10.1115/1.1345525

[19] A.F. Vakakis, Inducing passive nonlinear energy sinks in vibrating systems, Journal of Vibration and Acoustics Transactions of the ASME 123 (2001) 324-332. https://doi.org/10.1115/1.1368883

[20] X. Jiang, D.M. Mcfarland, L.A. Bergman, A.F. Vakakis, Steady state passive nonlinear energy pumping in coupled oscillators: Theoretical and experimental results, Nonlinear Dynamics 33(1) (2003) 87-102. https://doi.org/10.1023/A:1025599211712

[21] A.F. Vakakis, L.I. Manevitch, O. Gendelman, L. Bergman, Dynamics of linear discrete systems connected to local, essentially non-linear attachments, Journal of Sound and Vibration 264 (2003) 559-577. https://doi.org/10.1016/S0022-460X(02)01207-5

[22] O.V. Gendelman, E. Gourdon, C.H. Lamarque, Quasiperiodic energy pumping in coupled oscillators under periodic forcing, Journal of Sound and Vibration 294 (2006) 651-662. https://doi.org/10.1016/j.jsv.2005.11.031

[23] E. Gourdon, N.A. Alexander, C.A. Taylor, C.H. Lamarque, S. Pernot, Nonlinear energy pumping under transient forcing with strongly nonlinear coupling: Theoretical and experimental results, Journal of Sound and Vibration 300 (2007) 522-551. https://doi.org/10.1016/j.jsv.2006.06.074

[24] Y. Starosvetsky, O. V. Gendelman, Attractors of harmonically forced linear oscillator with attached nonlinear energy sink. II: Optimization of a nonlinear vibration absorber, Nonlinear Dynamics 51 (2008) 47-57. https://doi.org/10.1007/s11071-006-9168-z

[25] Y. Starosvetsky, O.V. Gendelman, Dynamics of a strongly nonlinear vibration absorber coupled to a harmonically excited two-degree-of-freedom system, Journal of Sound and Vibration 312 (2008) 234-256. https://doi.org/10.1016/j.jsv.2007.10.035

[26] M.A. Al-Shudeifat, N. Wierschem, D.D. Quinn, A.F. Vakakis, L.A. Bergman, B.F. Spencer, Numerical and experimental investigation of a highly effective single-sided vibro-impact non-linear energy sink for shock mitigation, International Journal of Non-Linear Mechanics 52 (2013) 96-109. https://doi.org/10.1016/j.ijnonlinmec.2013.02.004

[27] B. Fang, T. Theurich, M. Krack, L.A. Bergman, A.F. Vakakis, Vibration suppression and modal energy transfers in a linear beam with attached vibro-impact nonlinear energy sinks, Communications in Nonlinear Science and Numerical Simulation 91 (2020) 105415. https://doi.org/10.1016/j.cnsns.2020.105415

[28] Z. Lu, Z. Wang, Y. Zhou, X. Lu, Nonlinear dissipative devices in structural vibration control: A review, Journal of Sound and Vibration 423 (2018) 18-49. https://doi.org/10.1016/j.jsv.2018.02.052

[29] T. Yang, S. Hou, Z.H. Qin, Q. Ding, L.Q. Chen, A dynamic reconfigurable nonlinear energy sink, Journal of Sound and Vibration 494 (2021) 115629. https://doi.org/10.1016/j.jsv.2020.115629

[30] H. Ding, L.Q. Chen, Designs, analysis, and applications of nonlinear energy sinks, Nonlinear Dynamics 100 (2020) 3061-3107. https://doi.org/10.1007/s11071-020-05724-1

[31] S. Das, S. Tesfamariam, Y. Chen, Z. Qian, P. Tan, F. Zhou, Reliability-based optimization of nonlinear energy sink with negative stiffness and sliding friction, Journal of Sound and Vibration 485 (2020) 115560. https://doi.org/10.1016/j.jsv.2020.115560

[32] P. Alabuzhev, A. Gritchin, L. Kim, G. Migirenko, V. Chon, P. Stepanov, Vibration Protecting and Measuring Systems With Quasi-Zero Stiffness, Hemisphere Publishing, New York, 1989.

[33] R.A. Ibrahim, Recent advances in nonlinear passive vibration isolators, Journal of Sound and Vibration 314(3-5) (2008) 371-452. https://doi.org/10.1016/j.jsv.2008.01.014

[34] G. Gatti, M.J. Brennan, B. Tang. Some diverse examples of exploiting the beneficial effects of geometric stiffness nonlinearity, Mechanical Systems and Signal Processing 125 (2019) 4-20. https://doi.org/10.1016/j.ymssp.2018.08.024

[35] V.A. Bapat, P. Prabhu, Optimum design of a Lanchester damper for a viscously damped single degree of freedom system subjected to inertial excitation, Journal of Sound and Vibration 73 (1980) 113-124. https://doi.org/10.1016/0022-460X(80)90496-4

[36] M. Vakilinejad, A. Grolet, O. Thomas, A comparison of robustness and performance of linear and nonlinear Lanchester dampers, Nonlinear Dynamics 100 (2020) 269-287 https://doi.org/10.1007/s11071-020-05512-x

[37] A.D. Shaw, G. Gatti, P.J.P. Gonçalves, B. Tang, M.J. Brennan, Design and test of an adjustable quasi-zero stiffness device and its use to suspend masses on a multi-modal structure, Mechanical Systems and Signal Processing 152 (2021) 107354. https://doi.org/10.1016/j.ymssp.2020.107354.

[38] O. Zarraga, I. Sarría, J. García-Barruetabeña, F. Cortés, Dynamic analysis of plates with thick unconstrained layer damping, Engineering Structures 201 (2019) 109809. https://doi.org/10.1016/j.engstruct.2019.109809

[39] J.F.A. Madeira, A.L. Araújo, C.M. Mota Soares, C.A. Mota Soares, Multiobjective optimization for vibration reduction in composite plate structures using constrained layer damping, Computers and Structures 232 (2020) 105810. https://doi.org/10.1016/j.compstruc.2017.07.012

[40] A. Carrella, M.J. Brennan, T.P. Waters, Static analysis of a passive vibration isolator with Quasi-Zero Stiffness Characteristic, Journal of Sound and Vibration 301 (2007) 678-689 https://doi.org/10.1016/j.jsv.2006.10.011

[41] G. Gatti, Statics and dynamics of a nonlinear oscillator with quasi-zero stiffness behaviour for large deflections, Communications in Nonlinear Science and Numerical Simulation 83 (2020) 105143. https://doi.org/10.1016/j.cnsns.2019.105143

[42] G. Gatti, A K-shaped spring configuration to boost elastic potential energy, Smart Materials and Structures 28 (2019) 077002. https://doi.org/10.1088/1361-665X/ab1ec8

[43] X. Sun, X. Jing, Analysis and design of a nonlinear stiffness and damping system with a scissor-like structure, Mechanical Systems and Signal Processing 66-67 (2016) 723-742. https://doi.org/10.1016/j.ymssp.2015.05.026

[44] C. Gosselin, J. Angeles, Singularity analysis of closed-loop kinematic chains, IEEE Transactions on Robotics and Automation 6 (1990) 281-290. https://doi.org/10.1109/70.56660

[45] P.N. Liang, Screw-damper cover on a motorcycle primary-chain cover, Noise Control Engineering Journal 56 (2008) 478-483 http://dx.doi.org/10.3397/1.2987732

[46] G. Gatti, M.J. Brennan, Inner detached frequency response curves: an experimental study, Journal of Sound and Vibration 396 (2017) 246-254. http://dx.doi.org/10.1016/j.jsv.2017.02.008